Robot-assisted quasi-simultaneous laser welding of thermoplastics

The International Journal of Advanced Manufacturing Technology (2025) 138:2031–2042
https://doi.org/10.1007/s00170-025-15638-0

ORIGINAL ARTICLE

Robot-assisted quasi-simultaneous laser welding of thermoplastics

Manuela De Maddis[1,2] · Valentino Razza[1,2] · Dario Basile[1,2] · Khurshid Aliev[1,2] · Luigi Panza[1,2]

Received: 6 November 2024 / Accepted: 26 April 2025 / Published online: 9 May 2025

Abstract
The integration of robotics into quasi-simultaneous laser welding (QSLW) represents a significant advancement in materials joining technology, particularly for thermoplastics. This study explores the feasibility and effectiveness of employing a robotic arm in QSLW, a process traditionally carried out using galvanometric scanning heads due to its high-speed nature. The findings demonstrate that, through a robot-assisted process, it is possible to effectively control the meltdown level, a key parameter to ensure hermetic sealing, a typical requirement for this type of joint. This study identifies clamping force, welding speed, and laser spot size as the most significant parameters to achieve proper meltdown conditions at the weld interface. An experimental design, including an L9 orthogonal array and regression analysis, highlights the critical influence of these parameters on joint quality. A second-order regression model was developed to quantitatively describe the relationship between process parameters and material penetration at the interface, which is used as a representative indicator of the meltdown phenomenon. The model shows that the identified factors are mutually independent and, as a whole, accurately describe the behavior of the response variable, with a coefficient of determination exceeding 90%. The scope of this paper is to contribute to a deeper understanding of laser welding processes for thermoplastics, and to introduce a novel robot-assisted approach to QSLW, offering a reliable alternative to traditional galvanometric systems and demonstrating its capability to ensure both manufacturing efficiency and weld quality.

Keywords Quasi-simultaneous · Laser · Meltdown · Thermoplastics · Robotic welding

1 Introduction

In recent decades, the use of plastics has significantly increased, driven by their lightweight nature, flexibility, cost-effectiveness, and versatility, making them integral to industries such as construction, electronics, medicine, automotive, and even absorption media [1]. This growing industrial reliance on plastic components has heightened the demand for manufacturing processes that can offer greater flexibility, enhanced speed, and improved sustainability [2, 3].

In this context, innovative plastic welding methodologies have become essential, as they enhance production efficiency while ensuring the integrity and quality of finished products. Laser welding, particularly transmission laser welding (TLW) and quasi-simultaneous laser welding (QSLW) exemplify these characteristics [4]. TLW, which involves transmitting laser radiation through a transparent plastic component to an underlying absorbing component, offers several key advantages, including high energy efficiency, fast processing speeds, and precise control over welding parameters. This technique is particularly effective for joining polymers and thermoplastic components across a wide range of industries, delivering both precision and high-quality results [5, 6].

✉ Manuela De Maddis
manuela.demaddis@polito.it

Valentino Razza
valentino.razza@polito.it

Dario Basile
dario.basile@polito.it

Khurshid Aliev
khurshid.aliev@polito.it

Luigi Panza
luigi.panza@polito.it

[1] Department of Management and Production Engineering, Politecnico di Torino, C.so Duca degli Abruzzi 24, Torino 10129, Italy

[2] Advanced Joining Technologies Laboratory J-Tech@PoliTO, Politecnico di Torino, C.so Duca degli Abruzzi 24, Torino 10129, Italy

On the other hand, QSLW uses a predefined path that the laser beam traverses multiple times at very high scanning speeds, often facilitated by a galvanometer mirror system [7, 8]. Compared to TLW, QSLW results in more uniform heating, creating a weld that forms almost simultaneously along the entire joint line. This makes QSLW particularly suitable for components with complex geometries or large welding areas. When airtight welding and strong polymer bonding are required, both TLW and QSLW emerge as ideal processes [9]. In contrast to traditional welding methods, which typically apply thermal energy directly to the material surface, both TLW and QSLW specifically generate heat precisely at the interface of the two plastic components, enhancing efficiency and weld quality [10, 11].

However, these processes have limitations such as thickness constraints, the requirement for one laser-transparent and one absorbing part, and associated costs. Despite these limitations, the laser transmission-based welding process remains the preferred technology for joining thin thermoplastic shells containing electronic components, enabling joining without damaging delicate elements [12]. In both processes, the advantages include localized heating, rapid welding speed, absence of vibration, and reduced residual stresses [13].

For these processes, it is necessary to use the correct thermal input and apply pressure between the two joined parts. The pressure ensures close contact at the interface, which is essential for adequately conducting heat from the laser. In fact, without sufficient pressure, thermal energy may not be adequately transferred between components, leading to weak or incomplete joints. Mechanical clamps are commonly used to maintain this necessary pressure throughout the welding process, ensuring a uniform heat distribution and strong bonding across the interface [6, 8, 14, 15].

Indeed, to achieve a hermetic seal, an essential quality factor in both TLW and QSLW is the meltdown—the controlled collapse of the molten material at the interface. Proper meltdown ensures that the materials have fused adequately, creating a robust and hermetically sealed joint. If the meltdown is insufficient, the joint may lack strength, while excessive meltdown can cause defects and compromise the integrity of the weld [16]. Therefore, understanding the factors influencing meltdown is essential for optimizing the process [17].

The quasi-simultaneous welding technique has been analyzed in several studies, demonstrating its wide application in various industrial sectors. Ruotsalainen et al. [18] have investigated the QSLW of transparent thermoplastics. In particular, they have studied the joining of transparent polymers without absorbing additives, either between the two samples or by doping the polymer. Their comparative analysis between QSLW and the beam offset technique demonstrates that QSLW can consistently produce high-quality welds. Similarly, Ghasemi et al. [19] have examined the influence of various processing parameters—such as laser power, the number of passes, scanning speed, total scan length, and weld pressure—on meltdown during quasi-simultaneous laser welding of polycarbonate and polypropylene. By developing a model correlating these critical parameters, they have identified that the number of scans notably affects the extent of meltdown. Additionally, their findings indicate that increasing the laser power reduces induction time and simultaneously enhances both the meltdown rate and the overshoot. In contrast, because welding is primarily governed by the number of scans, increasing the scanning speed reduces both the total welding duration and the resulting meltdown. Furthermore, their study revealed that applying higher clamping pressure reduces the induction time needed for the welding process to initiate effectively. They have also established that total meltdown has a linear relationship with the total line energy input for polycarbonate and polypropylene. However, increasing the total scan length shifts the meltdown-line energy relationship downward, indicating that additional energy input becomes necessary due to thermal losses between successive scans. Indeed, increased heat conduction away from the weld area at longer scan lengths demands higher total line energy to achieve the desired meltdown. Complementing these findings, Jankus et al. [20] have explored how differences in polymer laser transparency affect joint quality during laser welding processes. In particular, they examine critical process parameters, such as laser power, scanning speed, and meltdown, to better understand their effects on joint quality. The study highlights how differences in laser transparency could significantly impact temperature distribution during welding through optical microscopy analysis of joint cross-sections combined with burst pressure tests. This variation in transparency has been found to cause non-uniform heating, resulting in heat-affected zones and the formation of pores. Additionally, the research identifies a direct correlation between cooling times during joint formation and the final amount of meltdown. Similarly, the authors in [21] have investigated how laser transmission welding and rib geometry parameters influence joint strength in injection-molded thermoplastic components. Their findings indicate that triangular rib geometries generally produce joints with higher strength than rectangular ones, emphasizing the significance of geometry optimization in enhancing welding conditions. Additionally, an analysis of rib dimensions demonstrated that joint strength increases proportionally with the width-to-height ratio—specifically, joints become stronger as the rib width increases or height decreases.

While these existing studies provide valuable insights into quasi-simultaneous laser welding techniques, they often do not thoroughly address the detailed aspects of joint quality, especially concerning meltdown dynamics critical for

achieving reliable hermetic sealing performance, particularly in robotic laser transmission welding applications. This work investigates using a robotic arm as an alternative to conventional scanning heads in QSLW of thermoplastic components. Initially, we perform a preliminary analysis to assess how key process parameters influence joint quality and to define appropriate variability ranges for each parameter. Then, we implement a systematic experimental design to investigate how these identified key process parameters, namely clamping force, laser spot diameter, and welding speed, affect the overall quality of the joint. Joint quality is evaluated primarily through its sealing performance, which depends directly on the extent of extruded molten material filling a specifically designed groove. Additionally, a regression analysis is conducted to quantitatively establish the relationship between these process parameters and the resulting meltdown behavior. This approach, combining structured experimental designs with regression modeling, aligns well with methodologies applied in similar welding research. For instance, Response Surface Methodology (RSM) has been effectively employed to link various laser parameters—such as peak power, welding speed, and pulse duration—to joint quality metrics in pulsed laser welding, demonstrating the advantages of statistically driven models for process optimization [22, 23]. Through this systematic investigation, the current study seeks to fill a critical gap concerning the understanding and effective control of meltdown dynamics within laser welding processes. Moreover, a robot-assisted approach to QSLW is presented as an alternative to traditional galvanometric systems, emphasizing its relevance to thermoplastic laser welding and its potential benefits in manufacturing efficiency and weld quality. This approach has proven effective in enabling precise control of process parameters, representing a promising solution for applications requiring high repeatability, joint integrity, and stringent quality standards.

Nomenclature

Δx (mm)	Material Penetration
Δz (mm)	Vertical Displacement from focal point
θ (mrad)	Divergence angle of the laser beam
D_L (mm)	Laser Spot Diameter
F (N)	Clamping Force
P_L (W)	Laser Power
u (J cm^{-1})	Laser Energy Density
v (mm s^{-1})	Laser Welding Speed
DoE	Design of Experiments
QSLW	Quasi-simultaneous Laser Welding
RMS	Response Surface Methodology
TLW	Transmission Laser Welding

2 Materials and methods

2.1 Experimental configuration and setup

This study examines two types of high-performance thermoplastics from UDEL®, a transparent and an opaque polysulfone polymer. These materials have high thermal performance, intrinsic flame resistance, strong chemical resistance, and excellent mechanical properties. UDEL polysulfone materials, which are amorphous resins, maintain their mechanical and thermal properties up to the glass transition temperature (T_g) of approximately 185 °C. The maximum recommended operating temperature is 150 °C. The material specifications used in this study are as follows: the transparent polysulfone polymer is UDEL P-3703, color NT 11; and the opaque polysulfone polymer is UDEL GF-120 Resin, reinforced with 20% glass fiber, color BK 973, providing higher rigidity, higher resistance to elevated temperatures, and a lower coefficient of linear thermal expansion. Table 1 summarizes the fundamental properties of the two polymers investigated. For both materials, the deflection temperature ranges between 174 and 180 °C under a 1.8 MPa load, and the extrusion temperature is between 315 and 370 °C [24].

The laser unit used is an LDF 4000-40 diode laser (Laserline, Mülheim-Kärlich, DE), delivering up to 4kW of power. The laser beam is delivered by a fixed optics OTS-5 (Laserline, Mülheim-Kärlich, DE) mounted on a 6-axis robot IRB 2400 (ABB, Zurich, CH). The laser has two parallel laser beams with wavelengths of 1020 and 1060± 10 nm, each delivering up to 2 kW of power. The laser spot diameter D_L^0 is 0.62 mm at a focal distance of 144 mm. The ABB robot controls the linear laser movement, which is defined by a custom procedure through ABB RobotStudio software. The specimen is manually positioned within a custom clamping system made of aluminum (see Fig. 1). This system con-

Table 1 Main properties of the thermoplastics used in the study

Property	UDEL P-3703	UDEL GF-120
Additives	None	20% glass fiber and black colorant
Density	1.24	1.40
Transition temperature, T_g (°C)	~185	~185
Processing temperature (°C)	329–385	343–399

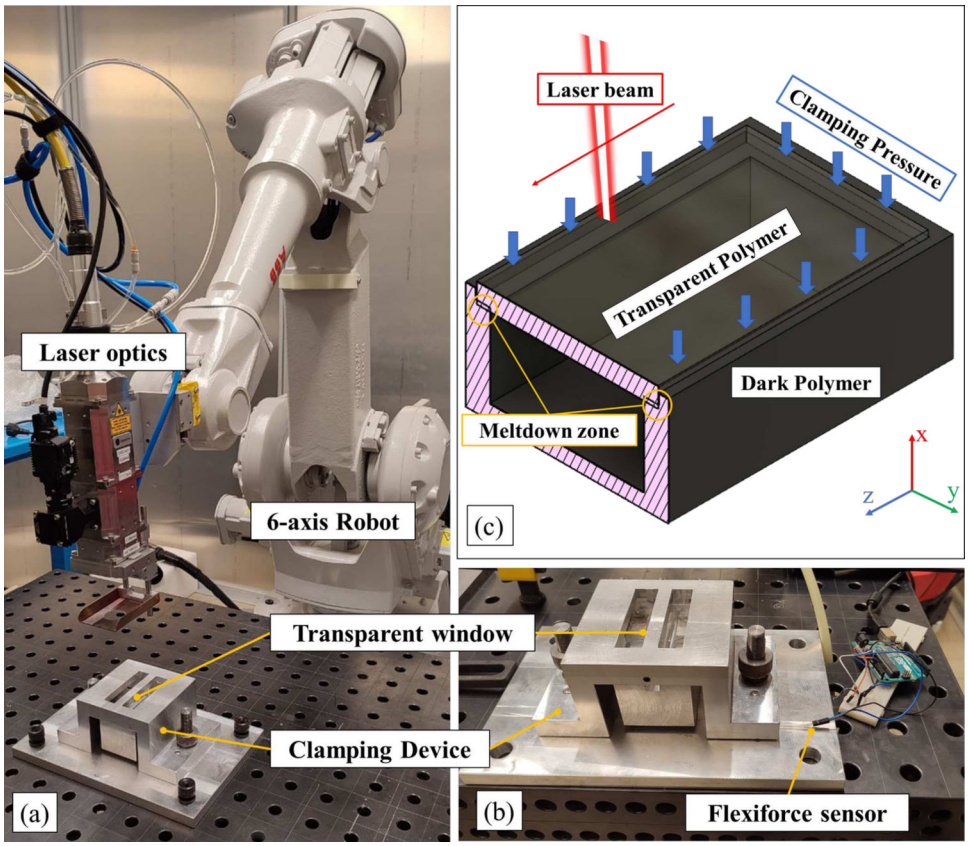

Fig. 1 **a** Experimental setup for quasi-simultaneous laser welding, **b** detail of the clamping device ensuring constant pressure, and **c** schematic of the welding process

sists of a fixture with a cavity perfectly accommodating the assembly. A bracket bolted to the table allows the assembly to be compressed using a laser-transparent glass retaining plate in contact with the transparent polymer. A constant pressure between the transparent and absorbing parts, a necessary condition for this process, is maintained by four springs positioned at the base of the fixture system. This setup ensures that constant pressure between the parts is guaranteed even if the assembly thickness changes during the process.

A FlexiForce load sensor (Tekscan, Boston, US) measures the clamping force applied during the experiments, converting the applied force into a change in electrical resistance. The FlexiForce sensor is wired in series with a 1 MΩ resistor to create a voltage divider, allowing the instantaneous measure of the resistance with a microcontroller. The force sensor is calibrated using a compression test machine (Easydur, Varese, IT). Figure 1b shows the sensor installed in the clamping device.

2.2 Joint inspection

We assess the weld quality through visual inspection of a cross-section under a microscope, correlating the measurement of the reduction in the assembly height due to the interpenetration of the two parts. The sample is cut along a plane perpendicular to the weld path (see Fig. 2). We ground and polish the surfaces of interest using a grinding machine to highlight the joint between the surfaces.

The cross-sectional images of the welding zone are captured using an Axio Vert.A1 optical microscope (Zeiss, Oberkochen, DE). We measure the displacement of the transparent part relative to the absorbing part with a micrometer. The displacement value is calculated as the average of three measurements taken along the section line (see Fig. 2). We also evaluate the difference Δx between the displacement before and after welding.

2.3 Preliminary analysis of the parameters affecting joint quality

We carry out a set of preliminary experiments to define the variation ranges of the primary process parameters used in the experiments. According to the literature, the critical parameters in plastic welding techniques are temperature, duration, and pressure (see, e.g., [10]). In laser welding, these parameters are controlled by laser power, welding speed, laser spot size, and clamping force [9, 25].

It is worth noting that the laser energy density (fluence), defined as the energy delivered per unit area, is commonly employed as a process parameter in terms of energy input. It captures the combined effects of three key factors: laser power P_L, which represents the thermal source capacity;

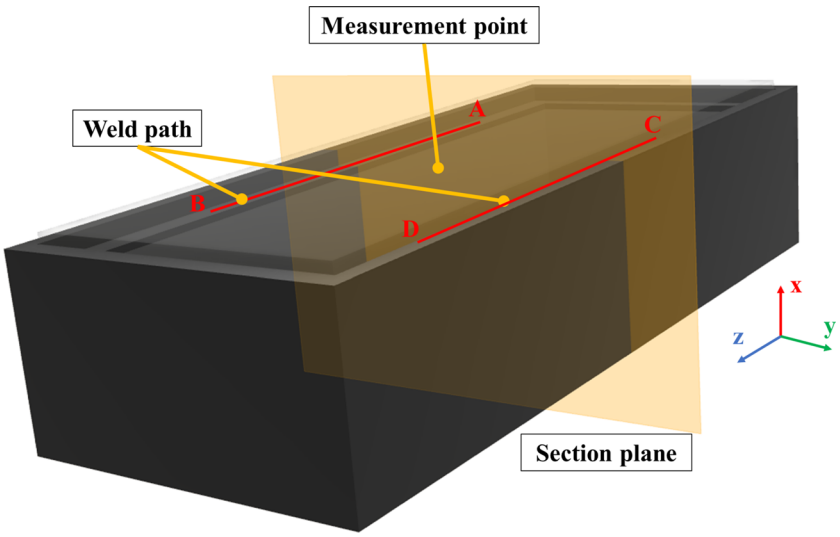

Fig. 2 Schematic representation of the weld path and the cutting plane for inspection

welding speed v, which governs the interaction time; and spot diameter D_L, which defines the area over which energy is applied to the material. Together, these factors influence the geometry and mechanical properties of the weld. Thus, the fluence, or energy density u, is directly proportional to the laser power and inversely proportional to both the welding speed and the spot diameter and can be defined as [26]

$$u = \frac{P_L}{v \cdot D_L}. \tag{1}$$

The resistance of the welding joint increases with the laser energy density, enhancing the material flow properties and facilitating the achievement of a hermetic seal. This holds only up to a critical value, beyond which the joint strength decreases due to material decomposition.

A clamping system exerts the welding pressure, ensuring consistent pressure between the parts throughout the welding process. If the pressure is insufficient, it can lead to inadequate contact between the parts, resulting in a weak weld.

In the present study, the analysis is limited to a simple welding path comprising two linear joints arranged in the sequence of AB-CD, repeated cyclically (see Fig. 2). This particular welding path reduces the variability factors, such as curvilinear paths used in industrial applications, which fall outside the scope of this work.

The laser duty cycle is shown in Fig. 3, where the laser is switched on to the selected power, moving from point A to B and from C to D, and switched off otherwise.

The laser power must be accurately selected to avoid incomplete fusion of the material, resulting in insufficient or incomplete laser penetration (see, e.g., [27, 28]) or excessive power transmitted to the object (see, e.g., [29]). As shown in Fig. 4c, an excessive value of the laser energy density leads to critical conditions, approaching the material decomposition temperature [7, 21].

The clamping force significantly influences the welding process. Even with correct laser positioning and power conditions, an insufficient force prevents proper joining [30,

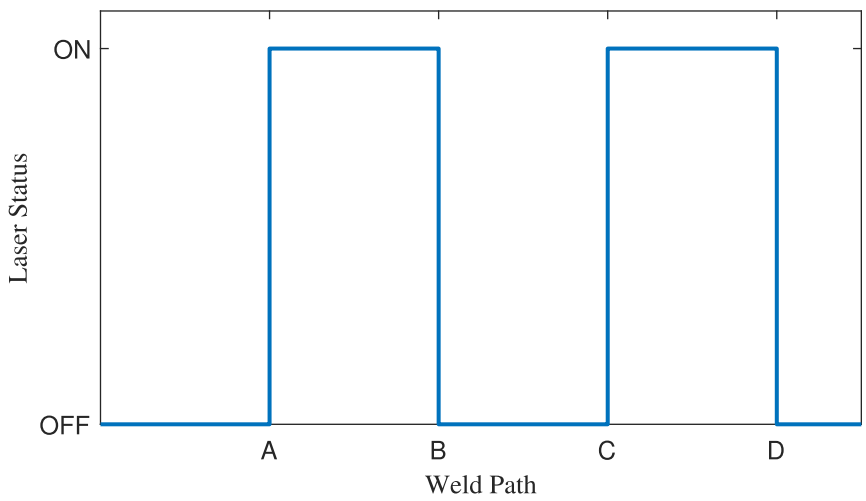

Fig. 3 Laser power duty cycle. State 1 represents the laser on status; 0 represents the laser off status

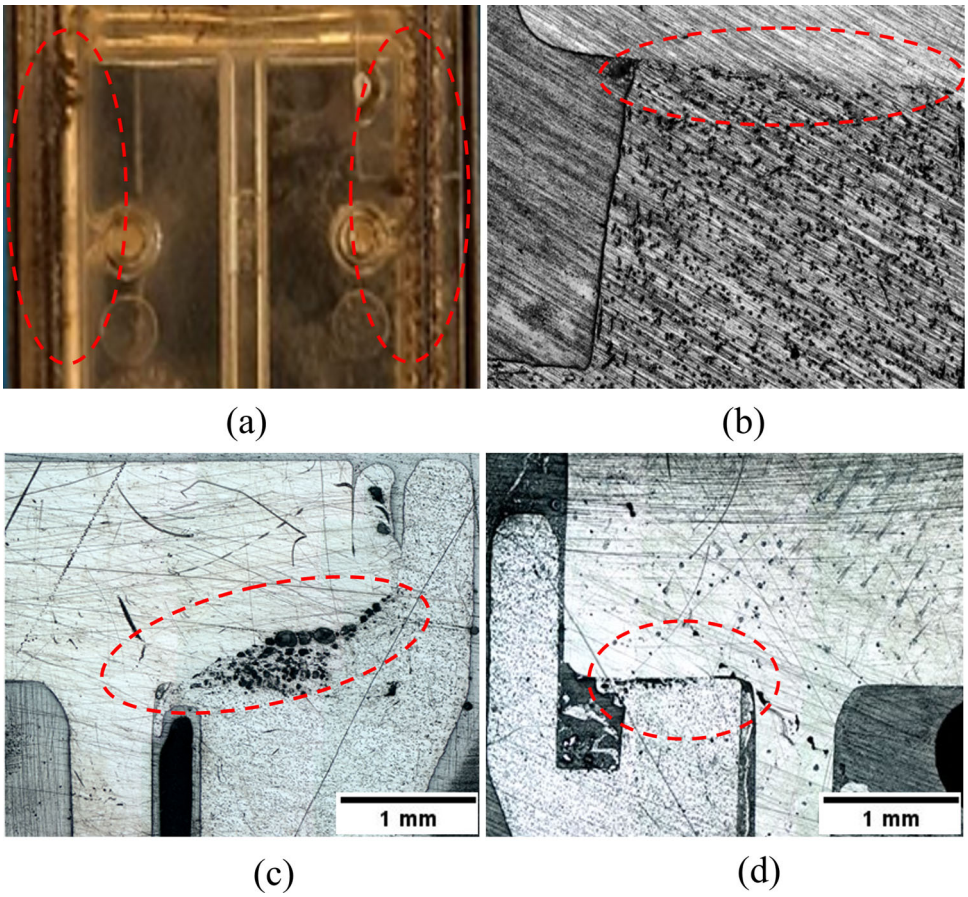

Fig. 4 Main defects in transmission laser welding: **a** surface burn marks, **b** lack of fusion, **c** excessive penetration, and **d** partial penetration

31]. As shown in Fig. 4b, even with adequate energy density, welding the components is impossible without sufficient force to keep them in contact.

The laser spot size D_L can be varied by adjusting the offset of the laser focus point according to

$$D_L = \sqrt{D_L^{0\,2} + \left(\Delta z \cdot \frac{\theta}{1000}\right)^2}, \tag{2}$$

where $D_L^0 = 0.62\,\text{mm}$ is the laser spot size at the nominal focal distance, Δz is the displacement from the focal distance, and θ is the divergence angle of the laser beam (325 mrad). The focusing distance may lead to a poorly shaped seam and incomplete penetration or transmission of the laser through the transparent polymer layer. Figure 4a depicts an example of welding carried out with the focus outside the absorbing part, resulting in a joint that is neither strong nor aesthetically acceptable.

We also study the influence of the number of scans. The results, depicted in Fig. 5, show how the penetration depends on the number of cycles, confirming the literature results [28, 32, 33]. Figures 5 and 6 show that, with all other process parameters held constant, increasing the number of cycles

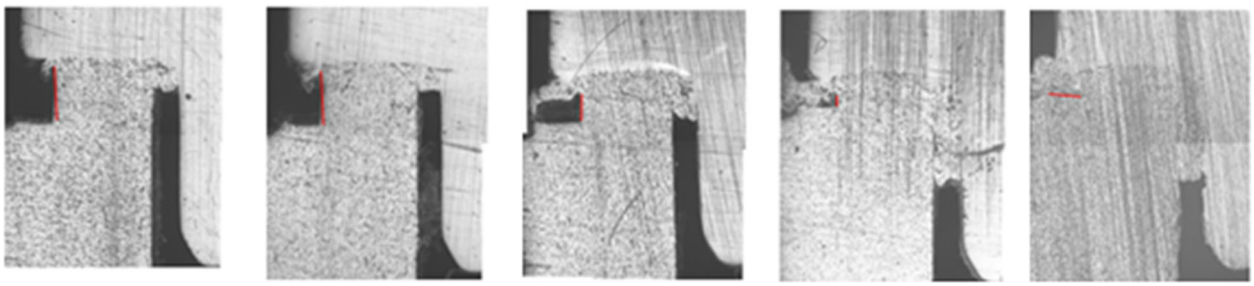

Fig. 5 Influence of the number of scans on penetration depth

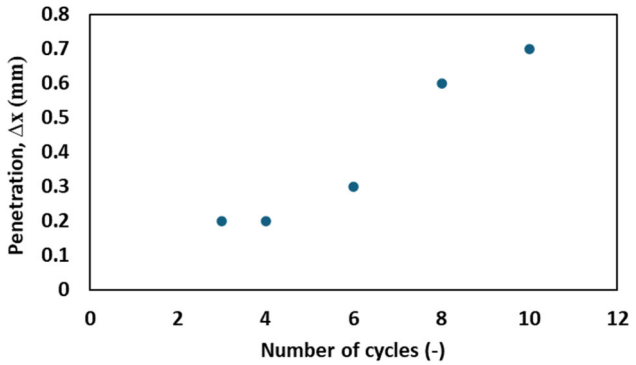

Fig. 6 Influence of the number of cycles on penetration

transitions the welding condition from non-welding to excessive melting and extrusion.

The defects and their potential corresponding causes are summarized in Table 2.

2.4 Selection of joint quality output variables

As the laser repeatedly passes over the joint area of the component, the polymer in the interface zone between the two parts begins to collapse. Due to the pressure exerted during the process, the molten transparent polymer flows into the cavity specifically designed in the dark polymer body (Fig. 7), ensuring an airtight seal. When the temperature reaches the polymer's melting point, the material at the interface begins to melt or soften significantly, initiating the meltdown [27]. This phenomenon continues until the cavity is filled, without affecting the geometry of the gap, as evidenced by Fig. 7. The meltdown causes interpenetration of the parts and, therefore, reduces the thickness of the assembly composed of a transparent cover and a dark body. The material penetration Δx has been chosen as the quality parameter to investigate, computed through the cross-sectional images of the welding zone during the joint inspections. In quasi-simultaneous laser transmission welding, where the temperature is increased uniformly or progressively across the joint interface, a complete meltdown can occur under proper conditions, guaranteeing a strong and durable weld.

Table 2 Defects and their causes

Defect	Cause
Surface burn marks	Incorrect focus position
Lack of fusion	Insufficient power density
Excessive penetration	Excessive power density
	Excessive number of cycles
Partial penetration	Insufficient clamping force

2.5 Design of experiments

We used the DoE analysis to understand how input variables—specifically the process parameters and their interactions—influence joint quality, as described by measured outputs.

The study focuses on the effects of clamping force F, welding speed v, and spot size D_L on joint quality, determined by material penetration Δx. The cross-sections of the joints are analyzed using an optical microscope to measure material penetration.

A factorial experiment has been performed to systematically examine the effects of multiple variables on the dependent variable. Specifically, we select the combinations of process parameters for the DoE according to the L_9 Taguchi design (also known as the orthogonal array) to evaluate the amount of meltdown as the quality criterion. One advantage of this technique is reducing the number of testing combinations, as it employs a fractional factorial design. This approach allows some combinations to be tested multiple times to assess their repeatability.

Before defining the Taguchi design, factors and levels of the process parameters were established. Three levels have been chosen for each of the aforementioned process parameters, and we replicate each test three times to ensure consistent results. Table 3 reports the levels of process parameters and the experimental design using the orthogonal array L_9.

3 Results and discussion

The experimental results have initially been qualitatively analyzed using main effect graphs to explore the relationships between the process parameters and the response variable, material penetration. This preliminary analysis provides valuable information on the individual influence of each process parameter on material penetration, confirming previous studies [9–11, 14] results. Subsequently, we perform a regression analysis to quantify these relationships further.

Main effect plots are graphical representations that illustrate the impact of each independent variable (process parameter) on the dependent variable (material penetration) while holding other variables constant at specified levels. In these plots, the x-axis represents the levels of the independent variable, and the y-axis shows the corresponding effect on the dependent variable. The line connecting the points on the plot demonstrates how changes in the levels of each process parameter affect material penetration. This visualization helps to understand the relative significance of each parameter within the experimental framework. Figure 8 shows the main effect plot.

The main effect plot illustrates the influence of three independent variables, i.e., the laser spot size, clamping force, and

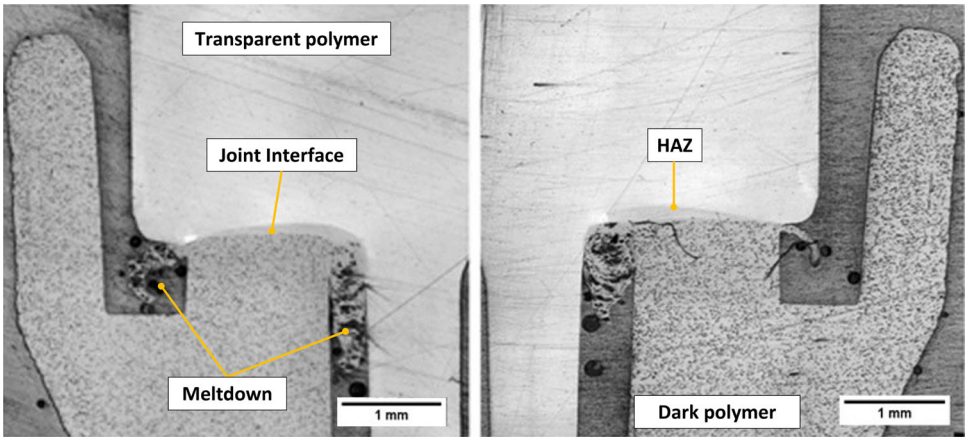

Fig. 7 Example of a sound weld with the proper amount of meltdown

welding speed, on the response variable, the material penetration. For the laser spot size, the mean response increases from level 1 to level 2, then decreases from level 2 to level 3, indicating that the middle level yields the highest mean response. This suggests a non-linear relationship between laser spot size and material penetration, as noted in earlier investigations [34].

In the case of clamping force, the mean response decreases significantly as the level increases, implying that higher clamping force leads to reduced material penetration, with the highest level resulting in the lowest mean response [30, 31].

For welding speed, the mean response decreases slightly from level 1 to level 2, then increases from level 2 to level 3, showing a non-linear relationship [35, 36].

Following this qualitative analysis, we perform a regression analysis to establish a more precise and quantitative relationship between the process parameters and material penetration. All the statistical analyses have been performed with Minitab software.

In its general form, a linear regression model is defined as

$$y = b_0 + b_1 h_1 + b_2 h_2 + \ldots + b_n h_n + \epsilon \tag{3}$$

Table 3 L_9 Taguchi-based Design of Experiments parameters values

Force (F), N	Speed (v), mm s^{-1}	Spot Size, D_L (mm)
60	500	1.68
60	550	1.92
60	600	2.17
80	500	1.92
80	550	2.17
80	600	1.68
100	500	2.17
100	550	1.68
100	600	1.92

where y is the dependent variable (material penetration), h_i are the independent variables, b_i are the estimated model parameters, and ϵ is the residual between the observed value and the predicted one.

Based on the results of the main effect plot, the regression analysis included all three process parameters and utilized a second-degree polynomial to capture the non-linear behavior previously observed graphically.

Model parameters are typically determined using the Ordinary Least Squares (OLS) method, which minimizes the sum of squared differences between observed and predicted values.

Various metrics are employed to assess the significance of the estimated model parameters. One such metric is the p-value from a two-sided hypothesis test, which evaluates whether there is a significant difference between a sample estimate and a hypothesized population parameter. If a model parameter p-value exceeds 0.05, the term is not considered significant at the 5% significance level, considering the other terms in the model.

Additionally, the confidence interval, which indicates the range of possible values for the model parameter at a given confidence level (typically 95%), is used. A narrower con-

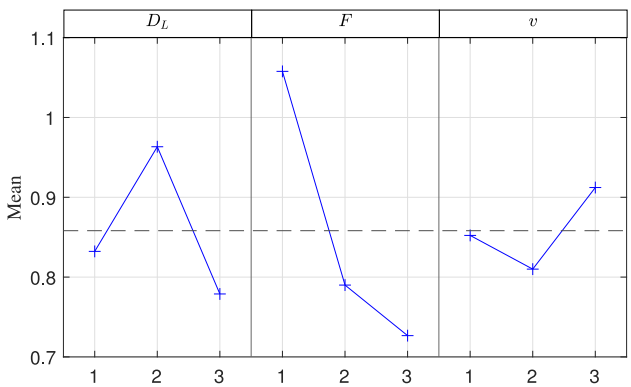

Fig. 8 Main effects plot for material penetration (Δx) as the response variable

fidence interval implies a more precise parameter estimate [37].

The regression equation obtained is

$$\Delta x = b_0 + b_1 D_L + b_2 F + b_3 v + b_4 D_L^2 + b_5 F^2 + b_6 v^2 + \epsilon \quad (4)$$

Table 4 reports the regression model coefficients estimated with the OLS method.

The regression model coefficients presented in Table 4 indicate that all the coefficients are statistically significant. The p-values for each coefficient are below the 0.05 threshold, confirming their significance. These results affirm the reliability of the model and the importance of each parameter in explaining the variability in the response variable.

Moreover, to evaluate the model goodness of fit, the coefficient of determination (R^2) is adopted, which quantifies how well the model explains the variance in the data

$$R^2 = 1 - \frac{\sum_{i=1}^{N} \epsilon_i^2}{\sum_{i=1}^{N} (\Delta x_i - \bar{\Delta x})^2} \quad (5)$$

where Δx_i is the i-th observed value, N is the number of observations, $\bar{\Delta x}$ is the arithmetic mean of the observed data, and ϵ_i is the residual, i.e., the difference between the observed data and the predicted value.

The coefficient of determination R^2 for the current regression model is 91.94%, showing a good level of approximation of the linear model to the measured data.

Finally, we verify that the underlying assumptions of the linear regression model are achieved. The first assumption is that the residuals are normally distributed, which is crucial for the validity of statistical inferences about the regression coefficients and predictions. Non-normally distributed residuals affect hypothesis tests, confidence intervals, and p-values. We check this assumption graphically, using a normal probability plot of residuals [38]. From the residual plot, shown in Fig. 9, we see that the residuals generally align with the reference line and follow a normal distribution. The points near zero residuals closely adhere to the line, suggesting that most data points fit the normal distribution well.

Table 4 Coefficient estimates of the regression model defined in Eq. 4

Coefficient	p-value	Estimate	95% Confidence Interval
b_0	< 0.001	1.238	[0.936, 1.540]
b_1	< 0.001	0.6044	[0.4051, 0.8038]
b_2	< 0.001	−0.5744	[−0.7738, −0.3751]
b_3	< 0.014	−0.2589	[−0.4582, −0.0595]
b_4	< 0.001	−0.1578	[−0.2071, −0.1085]
b_5	< 0.001	0.1022	[0.0529, 0.1515]
b_6	0.006	0.0722	[0.0229, 0.1215]

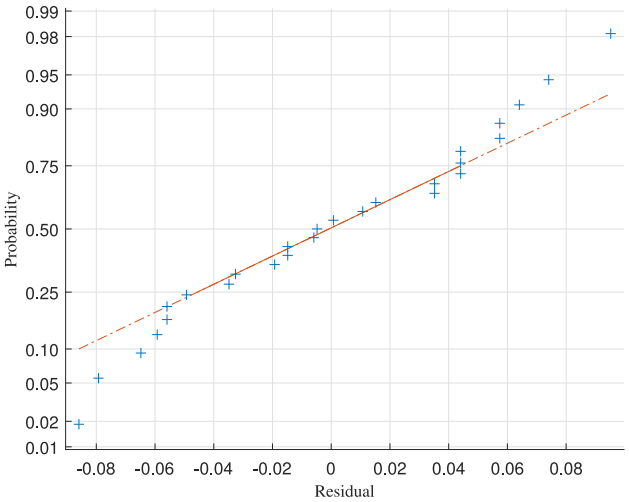

Fig. 9 Normal probability plot of residuals

However, there are some deviations at the extreme ends of the residuals, particularly on the left side (negative residuals) and, to a lesser extent, on the right side (positive residuals). These deviations suggest that the extreme values are not modeled by the normal distribution, which could indicate a slight departure from normality in the residuals at the tails. Overall, the plot supports the assumption of normal distribution for the residuals, with only minor deviations at the extremes. The second assumption is that the variance of the residuals is constant (homoscedastic) across all values of the independent variables. Homoscedasticity ensures that the error terms uniformly spread across the range of independent variable values. If this assumption is violated, it can lead to biased parameter estimates and incorrect confidence intervals. To visually assess homoscedasticity, plotting the

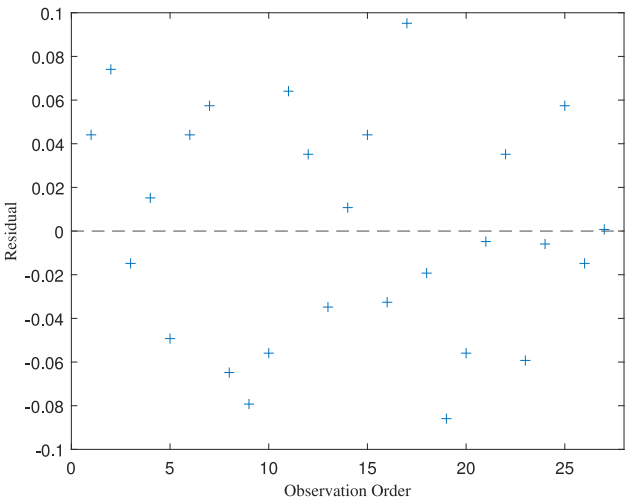

Fig. 10 Residuals versus Observation Order to check the homoscedasticity assumption

residuals against the observation order or fitted values is useful to identify anomalies.

Figure 10 shows that the residuals fluctuate randomly around the zero line, with no discernible pattern or trend across the observations. This randomness suggests that the residuals are independent of each other. Additionally, the spread of the residuals appears to be consistent across all observations, indicating that the variance of the residuals remains approximately constant throughout the experiments. There are no signs of increasing or decreasing variability, which supports the assumption of homoscedasticity. Overall, this plot confirms that the variance of the residuals is stable and consistent across the observations, which is a key assumption for the validity of the regression model.

4 Conclusions

This research successfully demonstrates the potential of robot-assisted quasi-simultaneous laser welding (QSLW) for thermoplastics, offering valuable insights into how key parameters, clamping force, welding speed, and spot size, impact meltdown phenomenon, which is crucial for the hermetically sealed joint. Integrating robotic arms in the welding process highlights advantages in achieving high precision, repeatability, and flexibility, especially for applications that require robust, hermetically sealed joints.

This study makes a meaningful contribution to the theoretical understanding of laser welding, particularly in the underexplored area of meltdown dynamics as a determinant of joint quality. A regression model is developed to quantitatively describe how key process parameters influence material penetration at the weld interface, serving as a reliable indicator of meltdown behavior. The results demonstrate that the selected parameters act independently and collectively accurately represent the system response, supported by a coefficient of determination greater than 90%. This predictive capability allows for precise control of the meltdown process based on specific parameter configurations. The proposed model thus lays a solid theoretical foundation for future developments in process analysis and optimization in the field of high-precision thermoplastic welding using robotic systems.

From a practical perspective, the results of this research have direct implications for manufacturers aiming to adopt the QSLW process using robotic arms to move the laser head as an alternative to traditional galvanometric systems. The study demonstrates the effectiveness of robotic arms in controlling the main process parameters, which have been identified as the most influential on the meltdown phenomenon.

The analysis focused specifically on meltdown, a topic still poorly explored in the literature but is a fundamental parameter to ensure proper hermetic sealing of the joint. This aspect is particularly relevant for thermoplastic components, where joining is often required to isolate the internal content from liquids or external environments, as demanded in various industrial applications.

This level of process control is crucial in industries where joint integrity and high production standards are essential requirements.

The insights this study provides enable manufacturers to refine their welding processes by acting directly on key parameters that directly impact joint quality and integrity.

Future research could build on these findings by validating the structural integrity of welded joints in practical applications involving more geometrically complex paths beyond just linear ones, thus examining how these geometries impact the quality of the melting process. This study could open up new possibilities for industrial applications.

Acknowledgements This study was supported by J-Tech@PoliTo, the Advanced Joining Technologies Research Center at Politecnico di Torino (http://www.j-tech.polito.it/). The authors thank Prof. F. Lombardi and Prof. P. Russo Spena from Politecnico di Torino for their valuable comments and insightful suggestions throughout the development of this work.

Funding Open access funding provided by Politecnico di Torino within the CRUI-CARE Agreement.

Data availability The authors attest that all data for this study are included in the paper.

Declarations

Competing interests The authors declare no competing interests.

References

1. Shamsuyeva M, Endres H-J (2021) Plastics in the context of the circular economy and sustainable plastics recycling: comprehensive

review on research development, standardization and market. Compos C Open Access 6:100168. https://doi.org/10.1016/j.jcomc.2021.100168
2. Skoczinski P, Krause L, Raschka A, Dammer L, Carus M (2021) Current status and future development of plastics: solutions for a circular economy and limitations of environmental degradation. In: Weber G, Bornscheuer UT, Wei R (eds) Enzymatic plastic degradation. Methods in enzymology, vol. 648. Academic Press, USA, pp 1–26. https://doi.org/10.1016/bs.mie.2020.11.001
3. Nguyen Q, Bagherzadeh SA, Parsian A, Akbari M, Karimipour A, Mosavi A (2021) Nonlinear model identification of dissimilar laser joining of S.S 304 and ABS using the Hammerstein-Wiener method. Optik 225:165649. https://doi.org/10.1016/j.ijleo.2020.165649
4. Vendan SA, Natesh M, Garg A, Gao L (2019) Confluence of multidisciplinary sciences for polymer joining. Springer, USA. https://doi.org/10.1007/978-3-030-14252-1
5. Jones I (2013) Laser welding of plastics. Woodhead Publishing, 280–301. https://doi.org/10.1533/9780857098771.2.280
6. Wu J, Lu S, Wang H-J, Wang Y, Xia F-B, Wang J (2021) A review on laser transmission welding of thermoplastics. Int J Adv Manuf Technol 116:773–789. https://doi.org/10.1007/s00170-021-07519-z
7. Jansson A, Kouvo S, Kujanpää V (2005) Quasi-simultaneous laser welding of polymers–the process and applications for mass-production. Proceedings of the International Congress on Applications of Lasers & Electro-Optics. https://doi.org/10.2351/1.5060516
8. Holtkamp J, Rösner A, Gillner A (2010) Advances in hybrid laser joining. Int J Adv Manuf Tech 47:923–930. https://doi.org/10.1007/s00170-009-2124-6
9. Acherjee B (2021) Laser transmission welding of polymers–a review on welding parameters, quality attributes, process monitoring, and applications. J Manuf Process 64:421–443. https://doi.org/10.1016/j.jmapro.2021.01.022
10. Gonçalves LFFF, Duarte FM, Martins CI, Paiva MC (2021) Laser welding of thermoplastics: an overview on lasers, materials, processes and quality. Infrared Phys Tech 119:103931. https://doi.org/10.1016/j.infrared.2021.103931
11. Kumar N, Bandyopadhyay A (2021) A state-of-the-art review of laser welding of polymers-part II: weld-quality studies. Weld J 100:100–114. https://doi.org/10.29391/2021.100.022
12. Maddock NA, James NL, McKenzie DR, Patrick JF (2012) Technological advances for polymers in active implantable medical devices. In: Davim JP (ed) The design and manufacture of medical devices. Woodhead publishing reviews: Mechanical engineering series, pp 239–272. Woodhead Publishing, UK. https://doi.org/10.1533/9781908818188.239
13. Gonçalves LFFF, Duarte FM, Martins CI, Paiva MC (2021) Laser welding of thermoplastics: an overview on lasers, materials, processes and quality. Infrared Phys Technol 119:103931. https://doi.org/10.1016/j.infrared.2021.103931
14. Acherjee B, Kuar AS, Mitra S, Misra D, Acharyya S (2012) Experimental investigation on laser transmission welding of PMMA to ABS via response surface modeling. Opt Laser Technol 44:1372–1383. https://doi.org/10.1016/j.optlastec.2011.12.029
15. Goyal D, Yadav R, Kant R (2022) An integrated hybrid methodology for estimation of absorptivity and interface temperature in laser transmission welding. Int J Adv Manuf Tech 121:795–808. https://doi.org/10.1007/s00170-022-09536-y
16. Prabhakaran R, Kontopoulou M, Zak G, Bates PJ, Baylis BK (2006) Contour laser transmission welding of glass reinforced nylon 6. J Thermoplast Compos Mater 19(4):427–439. https://doi.org/10.1177/0892705706066141
17. Amanat N, James NL, McKenzie DR (2010) Welding methods for joining thermoplastic polymers for the hermetic enclosure of medical devices. Med Eng Phys 32(7):690–699. https://doi.org/10.1016/j.medengphy.2010.04.011
18. Ruotsalainen S, Laakso P, Kujanpää V (2015) Laser welding of transparent polymers by using quasi-simultaneous beam off-setting scanning technique. Phys Procedia 78:272–284. https://doi.org/10.1016/j.phpro.2015.11.038. 15th Nordic Laser Materials Processing Conference, Nolamp 15
19. Gisario A, Veniali F, Barletta M, Tagliaferri V, Vesco S (2017) Laser transmission welding of poly(ethylene terephthalate) and biodegradable poly(ethylene terephthalate)-based blends. Opt Lasers Eng 90:110–118. https://doi.org/10.1016/j.optlaseng.2016.10.010
20. Jankus SM, Bendikiene R (2022) Effect of the meltdown on thermoplastic joint produced by quasi-simultaneous laser transmission welding. CIRP J Manuf Sci Technol 39:104–114. https://doi.org/10.1016/j.cirpj.2022.08.001
21. Bastos L, Alves M, Sousa B, Vilela A, Rietter L, Duarte F, Carneiro F, Żmijewska-Rocha A (2023) Transmission laser welding of thermoplastics: influence of welding parameters and rib dimensions on the strength of welded joints. J Adv Join Process 8:100173. https://doi.org/10.1016/j.jajp.2023.100173
22. Heydari H, Akbari M (2020) Investigating the effect of process parameters on the temperature field and mechanical properties in pulsed laser welding of ti6al4v alloy sheet using response surface methodology. Infrared Phys Technol 106:103267. https://doi.org/10.1016/j.infrared.2020.103267
23. Mosavi A, Soleimani A, Karimi A, Akbari M, Karimipour A, Karimipour A (2020) Investigating the effect of process parameters on the mechanical properties and temperature distribution in fiber laser welding of aisi304 and aisi 420 sheet using response surface methodology. Infrared Phys Tech 111:103478. https://doi.org/10.1016/j.infrared.2020.103478
24. Solvay specialty polymers: Udel polysulfone design guide. (2016). Solvay specialty polymers. Available at https://www.solvay.com/en/product/udel-polysulfone
25. Jansson A, Kouvo S, Salminen A, Kujanpää V (2003) The effect of parameters on laser transmission welding of polymers. In: Proceedings of the international congress on applications of lasers & electro-optics, pp 609–617. https://doi.org/10.2351/1.5060071
26. Franco A, Romoli L, Musacchio A (2014) Modelling for predicting seam geometry in laser beam welding of stainless steel. Int J Therm Sci 81:194–205. https://doi.org/10.1016/j.ijthermalsci.2014.01.003
27. Acherjee B (2021) Laser transmission welding of polymers–a review on welding parameters, quality attributes, process monitoring, and applications. J Manuf Process 64:421–443. https://doi.org/10.1016/j.jmapro.2021.01.022
28. Wippo V, Jaeschke P, Stute U, Kracht D, Haferkamp H (2012) The influence of carbon fibres on the temperature distribution during the laser transmission welding process. In: Proceedings of the European Conference on Composite Materials (ECCM)
29. Bates PJ, Okoro TB, Chen M (2014) Thermal degradation of pc and pa6 during laser transmission welding. Weld World 58:381–390. https://doi.org/10.1007/s40194-014-0209-9
30. Liu H, Jiang Y, Tan W, Wang X (2018) Enhancement of the laser transmission weldability between polyethylene and polyoxymethylene by plasma surface treatment. Materials 11(1):29. https://doi.org/10.3390/ma11010029
31. Chen Z, Huang Y, Han F, Tang D (2018) Numerical and experimental investigation on laser transmission welding of fiberglass-doped pp and abs. J Manuf Process 31:1–8. https://doi.org/10.1016/j.jmapro.2017.10.013
32. Acherjee B (2019) 3-D FE heat transfer simulation of quasi-simultaneous laser transmission welding of thermoplastics. J Braz Soc Mech Sci Eng 41(10):456. https://doi.org/10.1007/s40430-019-1969-3. All Open Access, Bronze Open Access

33. Jansson A, Kouvo S, Kujanpää V (2005) Quasi-simultaneous laser welding of polymers—the process and applications for mass-production. In: Proceedings of the international congress on applications of lasers & electro-optics, pp 801–810. https://doi.org/10.2351/1.5060516
34. Coelho JMP, Abreu MA, Rodrigues FC (2008) Modelling the spot shape influence on high-speed transmission lap welding of thermoplastics films. Opt Lasers Eng 46(1):55–61. https://doi.org/10.1016/j.optlaseng.2007.07.001
35. Acherjee B, Kuar AS, Mitra S, Misra D (2012) Modeling and analysis of simultaneous laser transmission welding of polycarbonates using an fem and RSM combined approach. Opt Laser Technol 44:1384–1393. https://doi.org/10.1016/10.1016/j.optlastec.2011.10.018
36. Jansson A, Kouvo S, Salminen A, Kujanpää V (2003) The effect of parameters on laser transmission welding of polymers. In: Proceedings of the international congress on applications of lasers & electro-optics, pp 609–617. https://doi.org/10.2351/1.5060071
37. Montgomery DC (2017) Design and analysis of experiments, 10th edn. John Wiley & Sons, Incorporated, New York
38. Panza L, De Maddis M, Russo Spena P (2022) Use of electrode displacement signals for electrode degradation assessment in resistance spot welding. J Manuf Process 75:93–105. https://doi.org/10.1016/j.jmapro.2022.01.060